ADVANCED FUNCTIONAL MATERIALS
www.afm-journal.de

Bioinspired Monopolar Controlled Ionic Hydrogels for Flexible Non-Contact Human–Machine Interfaces

Wenlong Wu, Tianyi Jiang, Min Wang, Tong Li, Yuxin Song, Jun Liu,* Zuankai Wang,* and Hongyuan Jiang**

Most flexible human–machine interfaces emulate the tactile system of the skin, which has the risk of contact damage. Additionally, contact deformation often leads to a hysteresis response. Non-contact interaction can address these problems. Inspired by the electroreception capabilities of the elephantnose fish, this study introduces a non-contact sensing model employing monopolar controlled ionic hydrogel. Compared to most existing mutual capacitive non-contact sensing models, this model not only boosts responsivity by over 3.5 times but also streamlines the sensing architecture. Utilizing this sensing model, a flexible non-contact human–machine interface is developed by organizing three differently shaped hydrogels into an asymmetric configuration. This device reliably discerns six non-contact gestures using machine learning algorithms and supports at least eleven interactive functions by detecting the duration of gestures, enabling continuous real-time control over external devices. This advancement heralds a more liberated paradigm of human–machine interaction with promising implications for the Internet of Things.

1. Introduction

The biological sensory system collects and transmits external stimuli to the nervous system as electrochemical pulses, which the brain then processes for feedback. Building on this foundation, various artificial sensory systems such as touch,[1–4] hearing,[5] taste,[6] vision[7] and olfaction[8] have been developed. These systems are vital for practical applications including wearable devices,[9,10] human–machine interfaces[11] and intelligent robots.[12–14] For flexible human–machine interfaces, the tactile sensory system offers an intuitive means for people to interact with computers and robots. This system primarily mimics the biological skin to response external contact and force via triboelectric effect,[15,16] piezoelectric effect,[17,18] piezoresistive effect,[19–21] piezocapacitive effect,[22,23] or their combination. However, the tactile sensory system has three drawbacks. First, the hysteresis phenomenon in the deformation process of the flexible material generates a hysteresis response in the sensor. Second, compulsive contact and pressure can generate inevitable contact damage. Finally, tactile interaction is confined to the interaction surface, limiting the potential and versatility of human hand motions. Consequently, there has been a growing demand for non-contact human–machine interfaces (NCHMIs). Most existing conventional NCHMIs rely on voice[24] or vision,[25,26] but they are hindered by drawbacks such as rigid structures and privacy limitations. Recent studies on flexible NCHMIs have primarily focused on integrating numerous triboelectric nanogenerators as sensing elements to achieve multiple interactive functions.[27–29] However, triboelectric nanogenerator-based NCHMIs can only recognize motion signals and lack the capability to continuously recognize stable gestures. This limitation prevents them from achieving stepless control of external devices. Moreover, the connection of a large number of rigid electrodes to the flexible sensing element will reduce its integrity and reliability. Therefore, the development of a simple, multifunctional, highly private, and flexible NCHMI is eagerly anticipated.

In the face of these needs, nature has tendered its answers. Many fish, including rays,[30] electric eels,[31] and elephantnose fishes,[32] possess electroreception abilities for non-contact interaction. The elephantnose fish, a representative of weakly electric fishes, has an electric organ in the caudal peduncle.[33] As shown in **Figure 1A**, each electrocyte is divided into a innervated face and a delayed response face. Under the control of the brain, the voltage-gated sodium channels on the innervated surface opens, and sodium ions enter the electrocyte, causing a positive action potential. After a delay, the sodium channels on the delayed response face opens, forming a negative action potential. Finally, stable emission of electric field is achieved during each electric

W. Wu, T. Jiang, H. Jiang
School of Mechatronics Engineering
Harbin Institute of Technology
West Da-zhi Street 92, Harbin 150001, P. R. China
E-mail: jty_hit@hit.edu.cn; jhy_hit@hit.edu.cn

W. Wu, M. Wang, T. Li, J. Liu
Department of Mechanical Engineering
City University of Hong Kong
Kowloon, Hong Kong 999077, P. R. China
E-mail: Jun.Liu@cityu.edu.hk

Y. Song, Z. Wang
Department of Mechanical Engineering
The Hong Kong Polytechnic University
Hong Kong 999077, P. R. China
E-mail: zk.wang@polyu.edu.hk

The ORCID identification number(s) for the author(s) of this article can be found under https://doi.org/10.1002/adfm.202408338

DOI: 10.1002/adfm.202408338

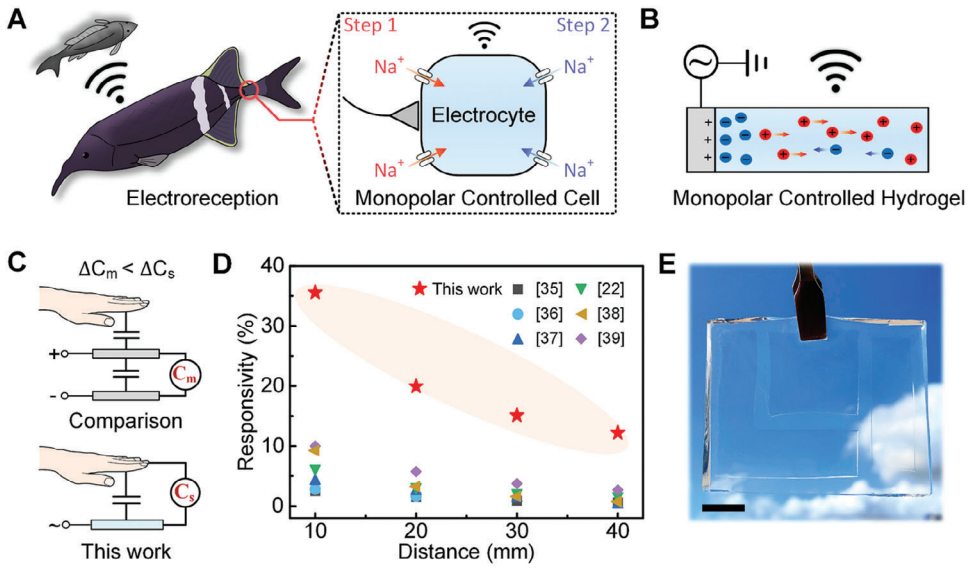

Figure 1. Concept and structure of bionic non-contact human–machine interface. A) Illustration of the elephantnose fish to achieve non-contact sensing. B) Elephantnose fish inspired monopolar controlled ionic hydrogel. C) Difference of working mode between this work and existing mutual capacitive sensors. D) Comparison of the responsivity of this work with the mutual capacitive sensors at 10–40 mm. E) Photograph of the asymmetric sensing array for non-contact human–machine interaction (scale bar: 10 mm).

organ discharge (EOD).[34] Due to the constant EOD, the resulting electric field creates a unique spatial voltage pattern on the skin surface of elephantnose fish that changes when external objects such as obstacles and predators are present. Then, elephantnose fish can use specialized electrosensory organs to detect minute changes in the electric field, which are then processed by the brain to provide feedback on the relative location of external objects and the fish.

Inspired by the elephantnose fish, this research proposes a non-contact sensing model using monopolar controlled ionic hydrogels, as illustrated in Figure 1B. Emulating the EOD, this model uses a drive signal generator in a single-electrode configuration to pulse the ion transfer in the ion-conducting hydrogel, generating a stable electric field around the hydrogel. When the hand is proximate to the hydrogel, it affects the electric field in the form of capacitance. This work further designs a customized PCB to mimic electrosensory organs, amplifying and collecting the affected electrical signals. In place of the brain, a machine learning algorithm analyzes changes in the electric field and provides feedback on the relative location between the hand and the hydrogel. Most of the sensing principles of capacitive flexible non-contact sensors are mutual capacitive sensors, as shown in Figure 1C. When the hand is close to the sensor, the capacitance between two electrodes is affected to achieve contactless sensing. However, the electric field generated by this sensing method is mainly constrained between the two electrodes, so the electric field emitted by the mutual capacitive sensor is weaker and has a smaller coverage range, which reduces the responsivity of non-contact sensing. For non-contact human–machine interaction, the control distance is typically greater than 10 mm. To establish a benchmark for comparison, this study evaluates signal responsivity at distances ranging from 10 to 40 mm. As shown in Figure 1D, the responsivity of the present model is more than 3.5 times that of the comparison models.[22,35–39] Additionally, the responsivity at a detection distance of 5 mm was also compared, as depicted in Figure S10 (Supporting Information). At shorter detection distances, the responsivity of mutual capacitive sensors has significantly improved, but it remains less than half of that observed in this work. Finally, based on the proposed monopolar controlled ionic hydrogel, this research constructs a hydrogel sensing array with an asymmetric pattern (Figure 1E) that can recognize six different non-contact gestures using just three external electrodes. When combined with gesture duration detection, a minimum of eleven interactive functions are attainable, as verified through the real-time wireless control of a drone using non-contact gestures. These findings underscore the significant potential of the NCHMI in human–machine interaction and the Internet of Things.

2. Results

2.1. Working Mechanism of the Monopolar Controlled Ionic Hydrogel

The non-contact spatial location electroreception ability of the elephantnose fish arises from the synergy between electric organs, electrosensory organs, and the nervous system. Consequently, the bionic NCHMI requires the development of an electric field generation module, a signal collection module, and a data processing module. During electrosensory processes, it is essential to generate an electric field using ion movement in the electrical organ. Ionic hydrogels are hydrophilic polymer networks that can store numerous water and ions. They possess tissue-like softness, and ions can move freely within the hydrogel, making them suitable for mimicking electronic organs.[40] In comparison to traditional hydrogels, double-network hydrogels exhibit significantly enhanced strength and stretchability due to the meticulous design of two interpenetrating networks. Thus, a sodium

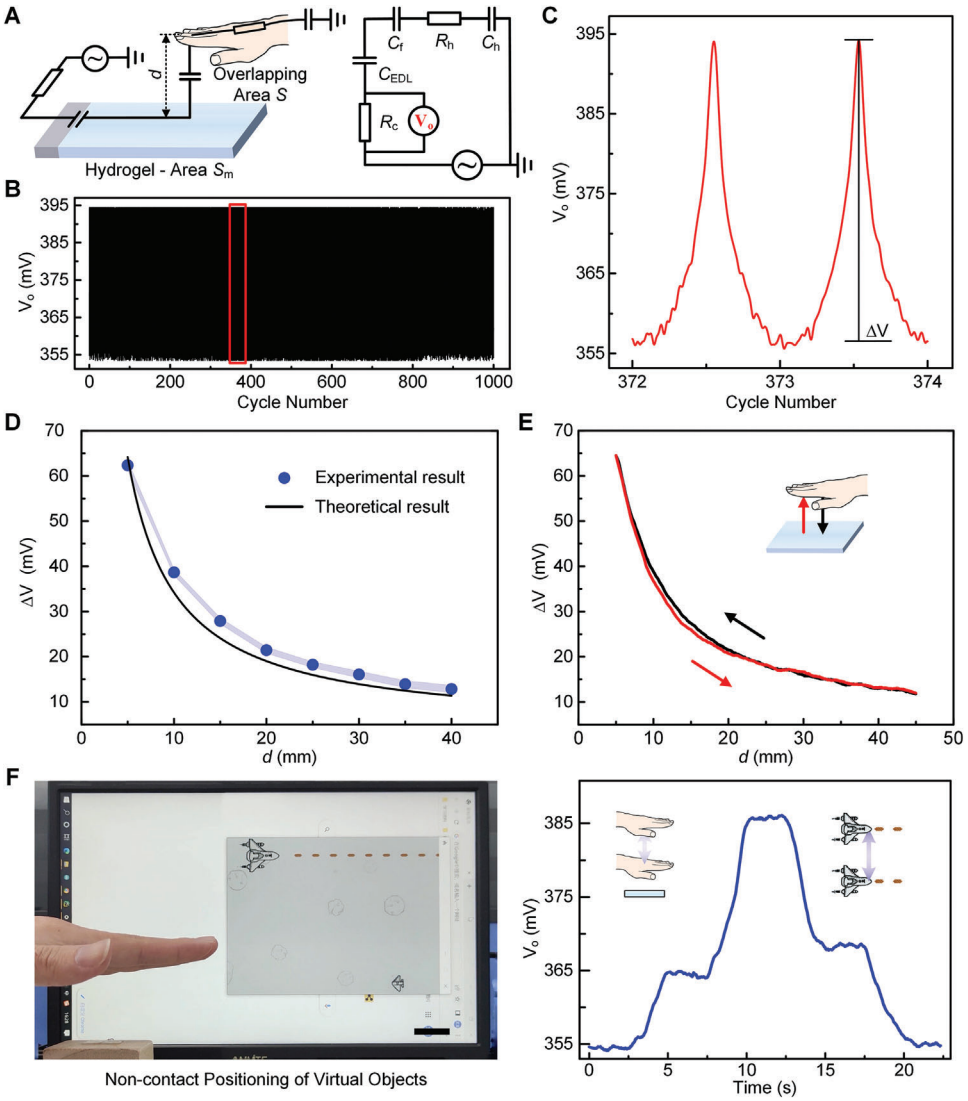

Figure 2. Principle and application of distance detection of monopolar controlled hydrogel. A) Equivalent circuit diagram of monopolar controlled hydrogel. B) Signal stability for 1000 cycles when the hand reciprocated at 10–150 mm from the hydrogel. C) Output voltage during the hand movement. D) The gesture voltage obtained by the empirical formula and experiments. E) Hysteresis of monopolar controlled hydrogel in 5–45 mm range. F) A monopolar controlled hydrogel was used to record hand height changes and control a computer game (scale bar: 10 mm).

alginate/polyacrylamide double-network hydrogel was synthesized to mimic electronic organs, demonstrating a satisfactory stretchability of 485% (Figure S11, Supporting Information). Additionally, the ion-conductive hydrogel was sandwiched between two stainless steel electrodes and measured using an electrochemical workstation (CHI660E) for electrochemical impedance spectroscopy (EIS). The hydrogel sample thickness was 1 mm, and the electrode diameter was 15.8 mm. As shown in Figure S12A (Supporting Information), the Nyquist impedance spectra show the relationship between the real and imaginary components of complex impedance of the hydrogel. At high frequencies, the intercept on the real axis represents the bulk resistance of the hydrogel, and the diameter of the semicircle indicates the charge-transfer resistance of the electrode.[41–44] The hydrogel displayed a satisfactory conductivity of 3.57 S m^{-1}, calculated using the equation $\sigma = L/SR$, where L corresponds to the thickness of the hydrogel, S corresponds to the effective overlap area, and R corresponds to the bulk resistance. Due to the high conductivity of the hydrogel, which reduces the resistance to charge transfer, there is no obvious semicircle in the Nyquist plot.

Figure 2A depicts the electric field generation process of the monopolar controlled ionic hydrogel, emulating the electric field production of the electric organ. The ionic hydrogel is connected to a high-frequency AC voltage generator through an auxiliary resistor and an electrode on one side. Ions within the hydrogel move with the alternating voltage, producing an electric field that extends infinitely. An equivalent circuit is proposed to facilitate analysis. In this circuit, an electric double-layer (EDL) capacitor forms between the electrodes and the hydrogel. When the hand is away from the hydrogel, the ionic hydrogel connects to the ground with an equivalent capacitance, which is connected in series with the electric double-layer capacitance. The capacitance

between the hydrogel and ground is referred to as the "initial capacitance." Furthermore, the effect of EDL is negligible due to its large capacitance and the high operating frequency.[45,46] The high conductivity of hydrogel also renders the resistance between the EDL and the grounded capacitor insignificant. When a hand is suspended above the hydrogel, the electric field is disturbed, and part of the electric field forms a field resembling that between parallel-plate capacitors. As a result, an equivalent capacitor forms between the hydrogel and the hand, connecting with the body resistor and the capacitor generated between the body and ground, replacing the initial capacitance. The equivalent parallel-plate capacitor is defined as a "gesture capacitor." During operation, changes in the electric field surrounding the hydrogel cause corresponding changes in the overall current of the loop. The loop current calculation process is presented in Text S1 (Supporting Information). Hence, the electric field changes can be reflected by the voltage across the auxiliary resistor.

In a typical experiment, the voltage response of the auxiliary resistor, reflecting changes in the electric field, was obtained and analyzed. Importantly, prior to participation in the experiments, informed consent was obtained from the volunteer in all experiments. For the hydrogel, electrochemical reactions are prevented when the voltage is maintained below 1 V.[47] Therefore, the peak voltage of the AC input signal was set to 1 V. The frequency of the AC input signal affects the circuit in two ways. On the one hand, it affects the impedance between the electrode and the hydrogel interface, and on the other hand, it influences the ability of the external environment to absorb the signal. When the applied frequency is less than 1 MHz, the Bode diagram of EIS (Figure S12B, Supporting Information) shows that there is a certain capacitance between the electrode and the hydrogel, which increases the impedance of the electrode and hydrogel interface and reduces the influence of gesture capacitance. As the frequency increases, the electric field is more easily absorbed by external environmental objects, further reducing the influence of gesture capacitance. The hydrogel was cut into cube with side lengths of 20 mm and a thickness of 1 mm. When the hand hovered 10 mm above the hydrogel, the changes in the output voltage at different frequencies were measured. As shown in Figure S2 (Supporting Information), a better output signal response was obtained when 1 MHz was used. Therefore, 1 MHz was selected as the frequency of the AC input signal. When the input peak voltage was 1 V and the frequency was 1 MHz, the hydrogel was moved up and down 1000 times with a distance of 1–15 cm from the hand, and the peak voltage of the auxiliary resistor was measured and shown in Figure 2B. When the distance between the hand and the hydrogel decreased from 15 to 1 cm, the voltage notably increased from 356.6 to 394.1 mV, as shown in Figure 2C. The signal output at this time consisted of noise and superimposed response signals. The noise signal, primarily influenced by the circuit and environment, remained constant during the signal output process. For the response signal, when the hand is distant from the hydrogel, it is considered the initial stage. At this time, the response signal is predominantly affected by the initial capacitance, and the output voltage signal is defined as the "baseline voltage." In contrast, when the hand is near the hydrogel, the response signal changes due to the influence of gesture capacitance, and the magnitude of the signal change is defined as "gesture voltage." If the ionic hydrogel is replaced with an electronic conductor as a sensitive element, a similar signal response would be observed under the same operating conditions. Sensing elements of the same size were fabricated using silver conductive paste, and their signal responses were recorded. As shown in Figure S13 (Supporting Information), the response signal amplitude was smaller compared to that of the ionic conductor. This may be because electrons are more constrained than ions in the presence of an external electrical signal. Therefore, when the hand is close to the sensitive element, the movement of ions inside the ionic conductor is more strongly disturbed, resulting in a more significant electrical signal response.

For the quantitative analysis of the gesture capacitance, which controls the gesture voltage, the traditional parallel-plate capacitance calculation formula $C = \epsilon S/d$ is inapplicable, as the distance between the hand and the hydrogel (d) is not significantly smaller than the facing area (S).[48,49] To further investigate the parameters affecting gesture capacitance changes and validate the accuracy of the equivalent circuit, both initial and gesture capacitances were calculated with the hand hovering at various heights above hydrogels of different sizes. The calculation process is detailed in Text S1 (Supporting Information). In the initial stage, the initial capacitance between the ionic hydrogel and ground exhibits a linear relation to the upper surface area of hydrogel (S_m). In the operating stage, part of the electric field forms capacitance with the hand. At this time, the gesture capacitance value is the sum of the initial capacitance (C_0) and capacitance changes (ΔC_f). The capacitance change is positively correlated with the ratio of the equivalent side length of the hand facing the hydrogel ($\sqrt{S}$) to the distance between the hand and the hydrogel (d). Consequently, the initial capacitance and capacitance change are fitted, with results displayed in Figure S4 (Supporting Information), indicating a good fit. Therefore, an empirical formula for gesture capacitance can be derived from this:

$$C_f = C_0 + \Delta C_f = aS_m + b\frac{\sqrt{S}}{d} + c \quad (1)$$

where a, b, c are constants. S_m is the upper surface area of hydrogel. S is the facing area between the hand and the hydrogel. d is the distance between the hand and the hydrogel. According to the empirical formula, the relationship between gesture voltage and distance can be obtained, as shown in Figure 2D. The experimental results show strong concordance with the theoretical results derived from the empirical formula.

To further verify the correctness of the empirical formula, the signal response of the hydrogel, which has an upper surface area of 400 mm^2 and a thickness of 1 mm, was collected when the distance between the hand and the hydrogel was less than 10 mm. The gesture voltage is shown in Figure S7 (Supporting Information). As the distance decreases, the gesture voltage increases significantly. The gesture voltage calculated using the empirical formula matches the experimental results well, further proving the accuracy of the empirical formula. Moreover, the empirical formula does not account for the effect of the hydrogel thickness on the signal response. This is because the thickness primarily affects the internal resistance of the hydrogel. Due to the high conductivity, changes in internal resistance have a smaller impact than changes in gesture capacitance impedance. When the upper surface area of the hydrogel is 400 mm^2 and the distance between

the hand and the hydrogel is 10 mm, the signal responses of hydrogels of different thicknesses were collected. The gesture voltage, shown in Figure S8 (Supporting Information), indicates that within the thickness range of 1–9 mm, the thickness of the hydrogel does not significantly affect non-contact sensing. Additionally, to assess the hysteresis characteristics of hydrogel-based contactless sensing, the position of ionic hydrogel remained static while the hand reciprocated at a uniform speed between 5 and 45 mm above it, with the corresponding gesture voltage variations captured in Figure 2E. Owing to the absence of physical deformation in the sensitive element during non-contact sensing, hysteresis response is virtually eliminated.

2.2. Performance of Distance and Facing Area Sensing

The empirical formula demonstrates that detecting alterations in the electric field surrounding the hydrogel can realize distance sensing and facing area sensing. For distance sensing, the elephantnose fish can determine its path according to the distance between an external object and itself. Correspondingly, in the field of human–machine interaction, distance sensing can be used for non-contact virtual object positioning. The computer recorded the output voltage as the hand moved over the hydrogel, and when the hand hovered over the hydrogel, the output voltage showed small fluctuations due to the shaking of the hand. When the hand ascended or descended, the output voltage decreased or increased respectively. These changes are positively related to the movement distance of the hand, as shown in Figure 2F. As shown in Movie S1 (Supporting Information), the movement distance of the hand is mapped to the computer game, and the aircraft can be controlled to evade enemy aircraft. However, playing computer games directly using distance mapping is challenging due to the high sensitivity of distance sensing and the difficulty in maintaining complete hand stability. When the control of the aircraft is based only on the hand movement direction, the controllable performance is more stable, as shown in Movie S2 (Supporting Information). Therefore, the above experiments indicate that the electroreception capability for distance can be emulated by detecting electric field changes around a single hydrogel to achieve non-contact positioning of virtual objects.

In addition to distance sensing, the elephantnose fish can also discern the relative position of external objects. Correspondingly, the monopolar controlled ionic hydrogel can detect the relative position by detecting the facing area. In the empirical formula, the influence of the hydrogel shape is not involved. To exclude the influence of the hydrogel shape on the output signal, hydrogels were shaped into I-shape, L-shape, and cube, which all possessing the same upper surface area of 400 mm^2 and a thickness of 1 mm. With the hand hovering at the same height above the differently shaped hydrogels, the gesture voltages and the corresponding calculated gesture capacitances were found to be similar in magnitude, as illustrated in Figure S9 (Supporting Information). These results are consistent with the empirical formula outcomes, suggesting that the hydrogel shape does not impact the gesture capacitance change when the hand entirely covers the hydrogel. To verify the effect of the facing area on the output signal, different numbers of fingers were hovered 10 mm above the 900 mm^2 hydrogel. The facing areas were estimated and substituted into the empirical formula, and the obtained gesture voltage is shown in **Figure** 3A. The experimental results are consistent with the calculation results of the empirical formula, confirming the accuracy of the equivalent circuit and the empirical formula. Therefore, the facing area can be calculated from the output voltage. When hydrogels form an array, the spatial relationship between the hand and the hydrogel array can be identified through the facing area between the hand and each hydrogel unit.

2.3. NCHMI Utilizing Monopolar Controlled Ionic Hydrogel Array and Applications

To achieve relative position identification through the detection of the facing area, analyses were conducted on different hydrogel array structures with the same area. As shown in Figure 3B, for the symmetrical structure, when the hand moves in the vertical or horizontal direction, the facing area of the hand and the hydrogel array also changes symmetrically. Therefore, for different hand positions, the facing area does not change significantly. For example, it is challenging for a hydrogel with a left-right bilateral symmetric layout to recognize whether the hand is on the left or right side of the hydrogel array. For asymmetric hydrogel arrays, when the hand is in different positions, the facing area changes greatly. Therefore, it is more conducive to the identification of the relative position of the hand. Taking the asymmetric layout of LOI as an example, three hydrogels with different shapes were encapsulated in silicone rubber to fabricate a hydrogel sensing array, achieving the construction of a NCHMI. Due to the excellent transparency and flexibility of both hydrogels and silicone rubber, the NCHMI displayed high transparency and deformability, as shown in Figures 3C and S14 (Supporting Information). The hydrogels with L-shape, O-shape, and I-shape were designated as hydrogel#1, hydrogel#2, and hydrogel#3, respectively, and their corresponding output voltages were named voltage 1 (V1), voltage 2 (V2), and voltage 3 (V3).

To detect changes in the electric field around the NCHMI, a customized PCB was designed, incorporating a microcontroller unit (Arduino Nano), a drive signal generator, and a processing circuit, as illustrated in Figure S15 (Supporting Information). The NCHMI and the customized PCB collectively emulate the electric organ and electrosensory organ of the elephantnose fish. Following this, the signals were gathered by a computer, as displayed in Figure 3C. In a typical experiment, the NCHMI was affixed to a horizontal work surface, and each of the three hydrogels within the NCHMI received the same drive signal from the generator, with a peak voltage of 1 V and a frequency of 1 MHz. Then, digital signals were collected by the computer as the hand hovered in various positions above the NCHMI. Owing to the differing areas of the three hydrogels, the baseline voltages varied. Figure S16 (Supporting Information) presents the gesture voltages of the three hydrogels to facilitate analysis. For example, when the hand was suspended in front of the NCHMI, the effective overlap areas of hydrogel#2 and hydrogel#3 were larger than that of hydrogel#1, resulting in higher gesture voltages for hydrogel#2 and hydrogel#3 compared to hydrogel#1. Similarly, the gesture voltages were positively correlated with the effective overlap areas when the hand was positioned above, behind, to the left or right of the NCHMI, or when a finger hovered over it. Due to

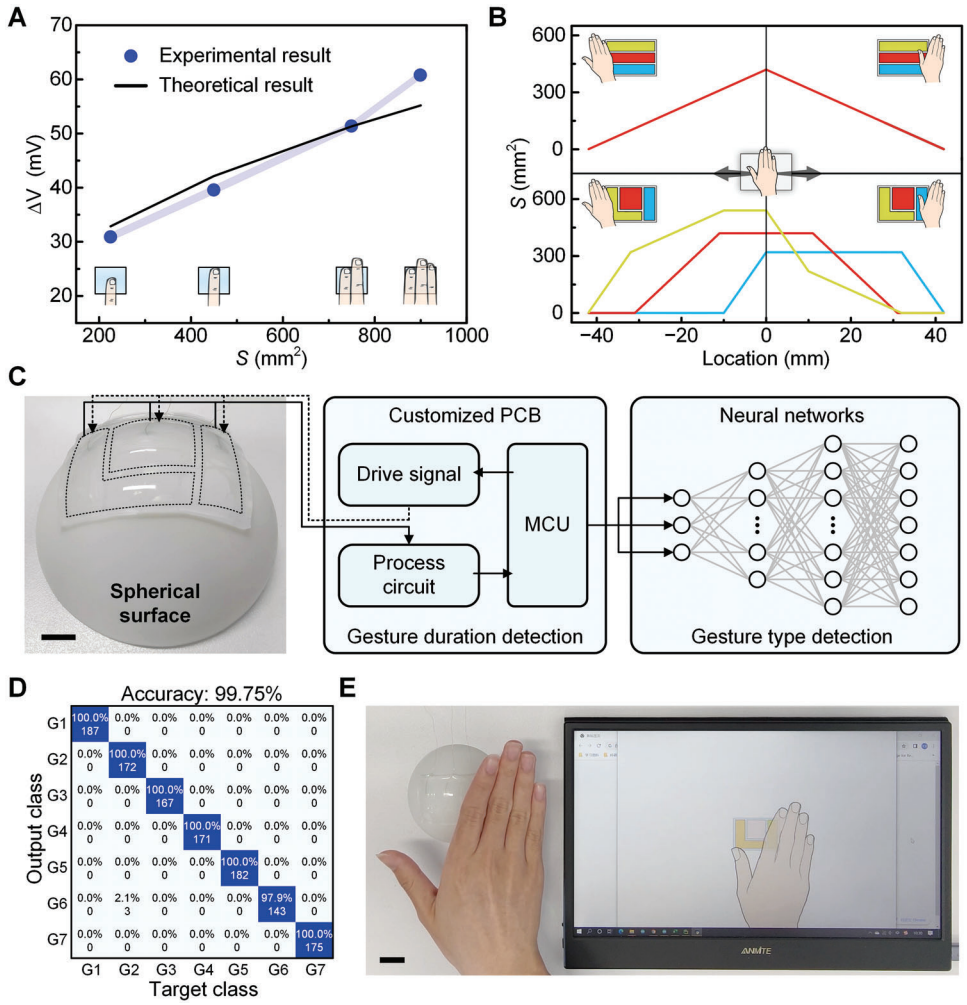

Figure 3. Non-contact gesture recognition based on facing area detection of monopolar controlled hydrogel. A) Gesture voltages obtained from empirical formula and experiments when a hand hovered at 10 mm from the hydrogel with varying facing areas. B) Variations in the facing area of each hydrogel within symmetric and asymmetric hydrogel arrays during hand movement. C) A schematic diagram of non-contact gesture recognition system (scale bar: 10 mm). D) Confusion matrix for non-contact gesture recognition. E) Visual display of non-contact gesture recognition (scale bar: 20 mm).

the inherent instability of the suspended hand, the gesture voltages fluctuated accordingly, potentially interfering with gesture recognition.

As elephantnose fish swim, the electric field surrounding their bodies becomes unstable. Despite this, they can accurately discern the relative locations of external objects. Analogously, achieving accurate and rapid identification of output signals is crucial for NCHMI. Traditional human–machine device analysis methods involve manually extracting shallow features, such as frequency and peak gap, which demand signal stability. Consequently, this method is weak in maintaining accuracy when the electric field changes. Due to the satisfactory performance of deep learning on coping with many groups of data, it has become a very popular subset of machine learning.[50–52] Therefore, as shown in Figure 3C, a neural network was constructed by Python for signal feature extraction and automatic gesture recognition, mimicking the function of the elephantnose fish brain. This neural network included one input layer, two hidden layers, and one output layer. Among them, the input layer contained three nodes, which were used to import three output voltages of NCHMI, respectively. The first hidden layer had nine nodes while the second hidden layer had 21 nodes. In addition, the activation function of each node in the hidden layer was Leaky ReLU. For signal classification, the activation function of the output layer was Softmax and seven nodes in this layer corresponded to seven touchless gestures. Gesture.1 represented the gesture when the hand away from the NCHMI. Gesture.2-5 represented the gestures when the hand suspended in front of, behind, left and right of the NCHMI, respectively. Moreover, Gesture.6 and Gesture.7 represented the gesture when the hand or a finger hovered above the NCHMI, respectively. Furthermore, Gesture.1-7 were named None, Front, Back, Left, Right, Hover and Point, respectively.

To verify the machine learning algorithm can simulate the elephantnose fish brain for the recognition of non-contact gestures under deformation, the output voltages in different touchless gesture modes were collected when the NCHMI was attached to different shaped working surfaces. At this point, the NCHMI deformed slightly to fit the different shaped surfaces. As shown

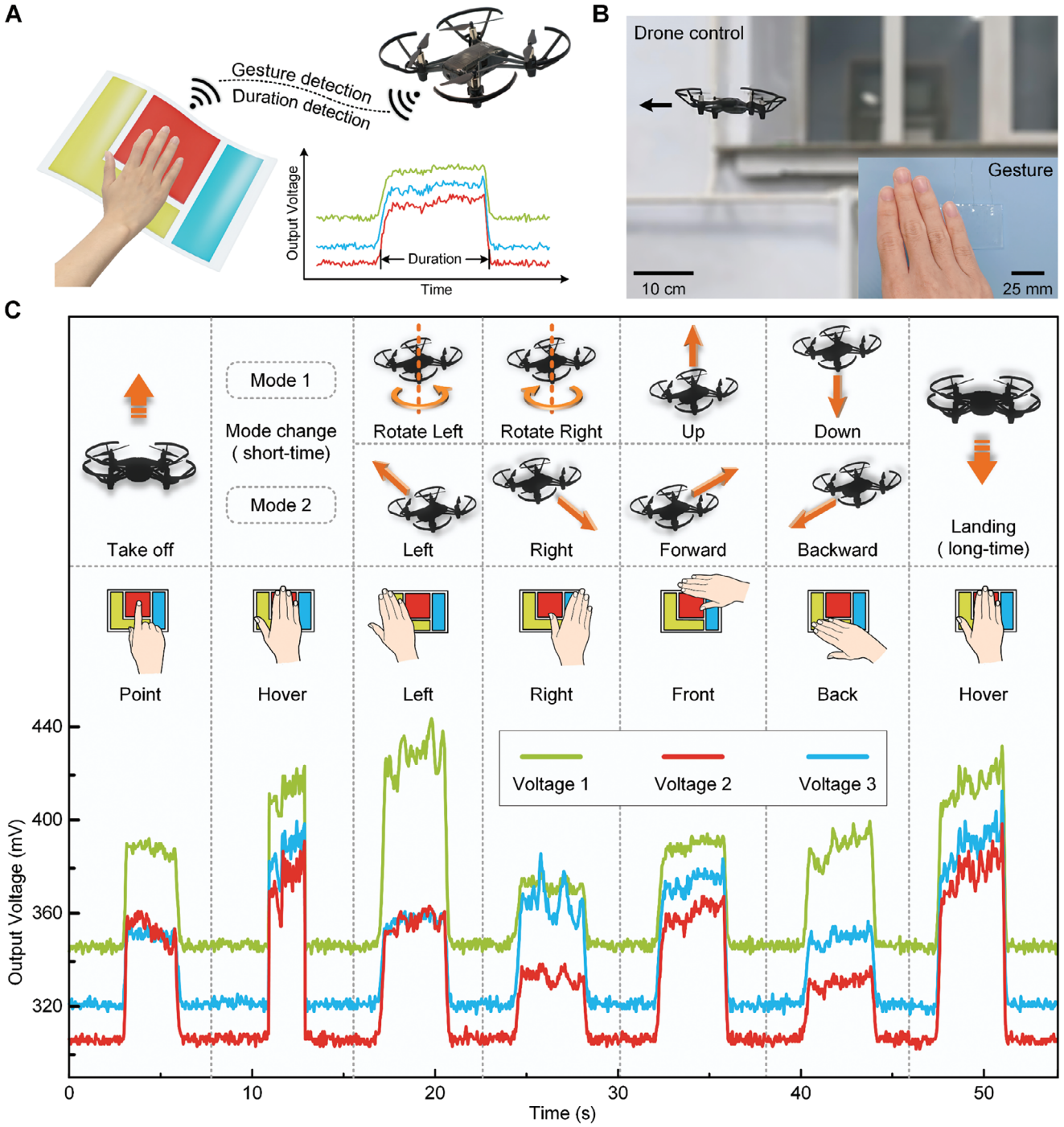

Figure 4. Demonstration of the NCHMI for drone control. A) Schematic diagram of the NCHMI controlling drone flight through both gesture detection and duration detection. B) Photo of wirelessly controlling a drone using touchless gestures through the NCHMI. C) Variations in output voltages and drone movements in response to different touchless gestures.

in Figure S17 (Supporting Information), when the work surface changed from horizontal surface to wavy and spherical surface, the initial capacitor varied. In addition, the height and effective overlap area between the hand and three hydrogels were different in the same gesture mode when the NCHMI was attached on various work surfaces. Therefore, the relationship of gesture voltages between different gesture modes changed. On each working surface, 6000 groups of output voltages in different gesture modes were collected. Among them, 80% of the data was used as the train set while the remaining data was used as the test set. As shown in Figures 3D and S17 (Supporting Information), over 99% accuracy can be achieved regardless of the working surface,

proving the DL actually achieves a high test accuracy rate. However, this accuracy was only for a specific dataset and cannot fully represent the real applications. Thus, the real-time demonstration of identification was shown in Movie S3 (Supporting Information), which verifies the DL can help NCHMI achieve accurate non-contact gesture recognition (Figure 3E). Furthermore, when the deformation of the NCHMI reached 50%, its gesture recognition ability was tested. To facilitate observation, silicone rubber and hydrogel were dyed. At this time, the coated silicone shell was significantly deformed and torn at the edges, limiting the further deformation of NCHMI. The output voltages in different touchless gesture modes were collected, as shown in Figure S18 (Supporting Information). It could be seen that the distribution of the response signal was similar to that when NCHMI was placed on a horizontal surface. However, due to the tensile deformation, the upper surface area of the hydrogel increased, so the response signal also increased. In the deformed state, DL could still achieve an accuracy of more than 99%, as shown in Figure S18 (Supporting Information). Moreover, a demonstration of real-time gesture recognition of NCHMI in a stretched state was shown in Movie S4 (Supporting Information), proving that NCHMI was still effective under large deformation conditions.

Since the NCHMI can output continuous signals, more interactive functions can be realized by detecting the duration of different gestures. As shown in **Figure** 4A, the flight of the drone can be collaboratively controlled through both gesture type and gesture duration. The drone has ten movements: take off, left, right, forward, backward, up, down, left rotation, right rotation, and landing. A pulse signal-based human–machine interface would require ten distinct gestures, while only six are needed through the collaborative control of gesture type and gesture duration. Furthermore, as shown in Figure 4B, the flight trajectory of the drone is consistent with the direction of the gesture, facilitating more intuitive and straightforward interactions. Specifically, as shown in Figure 4C, when a point gesture appeared, the drone took off. Subsequently, a brief Hover gesture enabled the switching of the flight mode of drone. In mode 1, left and right gestures corresponded to the drone rotating left and right, respectively, while front and back gestures controlled upward and downward movement. In contrast, mode 2 assigned Left and Right gestures to lateral movement, and Front and Back gestures to forward and backward motion. Lastly, a prolonged Hover gesture triggered the landing. The control logic of the NCHMI was simple and intuitive. Despite significant fluctuations in output voltage during operation, each gesture was accurately recognized, facilitating seamless drone control, as demonstrated in Movie S5 (Supporting Information).

3. Conclusion

Drawing inspiration from the elephantnose fish, this study introduces a non-contact sensing model for the monopolar controlled ionic hydrogel. This model serves as the foundation for developing a NCHMI, paired with a control circuit and machine learning algorithms, that enables continuous, real-time control of external devices without physical contact. The working mechanism is clarified, including an equivalent circuit for the non-contact sensing model and an empirical formula, both substantiated through experimental validation. This sensing model emulates the ability of the elephantnose fish to generate a stable weak electric field through ion transport and to detect the spatial position of external objects, even under deformation. Compared to mutual capacitive sensors, the monopolar controlled ionic hydrogel not only enhances the responsivity by more than 3.5 times, but also simplifies the sensing architecture. Based on this sensing model, a hydrogel sensing array with an asymmetric pattern is constructed to fabricate the NCHMI, which can identify both non-contact gestures and their duration. The integration with machine learning algorithms allows the NCHMI to stably recognize changes in non-contact gestures even when deformed. Thus, the NCHMI can adhere to various work surface shapes and adapt to different working environments. The improved NCHMI can recognize six distinct touchless gestures, provides eleven wireless interactive functions using just three external electrodes. Moreover, due to its non-contact sensing approach, the NCHMI exhibits virtually no hysteresis response. Experimental results demonstrate the NCHMI can wirelessly control external devices through non-contact gestures. The proposed NCHMI has potential applications in public electronic devices, reducing both contact damage and the risk of viral transmission. Furthermore, touchless interaction strategies enhance the efficiency and appeal of human–machine interactions, substantially promoting the development of the Internet of Things.

4. Experimental Section

Materials: Acrylamide (AM; 99.0%), *N,N'*-methylenebisacrylamide (MBAA), sodium alginate (SA), sodium chloride (NaCl), and calcium chloride were obtained from the Aladdin Industrial Corporation. 2-Hydroxy-2-methylpropiophenone (Irgacure 1173) was purchased from Sigma-Aldrich. Silver conductive paste was purchased from Shenzhen Xinwei New Materials Co., Ltd. All reagents were used without further purification.

Synthesis of PAM/SA Hydrogel: An SA/polyacrylamide (PAM)/NaCl double-network hydrogel was synthesized using a mold casting method. First, SA (0.7 wt%) and NaCl (5 wt%) were dissolved in deionized water (76.146 wt%). After that, AM (18 wt%), MBAA (0.054 wt%), and Irgacure 1173 (0.1 wt%) were dissolved in the previous solution to form a pre-gel solution. Next, the pre-gel solution was added into a mold and then irradiated with UV (wavelength:365 nm, intensity: 20 W) for 10 min to polymerize the AM into PAM. Finally, the hydrogel was soaked into a calcium chloride solution (2.5 wt%) for 5 min, crosslinking the alginate by the calcium ions to generate the second network.

Fabrication of the Conductive Paste-Based Sensing Element: The silver conductive paste was filled into the silicone mold and dried at 100 °C for 30 min to complete the preparation.

Fabrication of NCHMI: The NCHMI was fabricated using a four-step method. First, the required amounts of silicon oil (500 cSt) and components A and B of a silicone rubber were dispensed in a mixing container (1.25:1:1 by weight). The blend was mixed thoroughly for 5 min, then degassed under vacuum in a desiccator for 30 min. Second, the blend was poured into a cubical PMMA mold and then solidified partially by heating up to 70 °C for 12 min. Third, three hydrogels with different shapes were placed on the semi-cured silicone rubber substrate. Meanwhile, copper wires were placed under the hydrogels as electrodes. Finally, the silicone rubber mixture was poured over the hydrogels and allowed to set for 12 h to form the NCHMI.

Supporting Information

Supporting Information is available from the Wiley Online Library or from the author.

Acknowledgements

This work was financially supported by the National Natural Science Foundation of China (No. 12302352, No. 11872165), the China Postdoctoral Science Foundation (No. 2023M730867), and the Heilongjiang Provincial Postdoctoral Science Foundation (No. LBH-Z23018).

Conflict of Interest

The authors declare no conflict of interest.

Data Availability Statement

The data that support the findings of this study are available in the Supporting Information of this article.

Keywords

flexible sensor, human–machine interface, ionic hydrogel, nature inspired engineering, non-contact gesture recognition

Received: May 15, 2024
Revised: July 30, 2024
Published online:

[1] S. Chun, J.-S. Kim, Y. Yoo, Y. Choi, S. J. Jung, D. Jang, G. Lee, K.-I. Song, K. S. Nam, I. Youn, D. Son, C. Pang, Y. Jeong, H. Jung, Y.-J. Kim, B.-D. Choi, J. Kim, S.-P. Kim, W. Park, S. Park, *Nat. Electron.* **2021**, *4*, 429.
[2] H. Tan, Q. Tao, I. Pande, S. Majumdar, F. Liu, Y. Zhou, P. O. A. Persson, J. Rosen, S. van Dijken, *Nat. Commun.* **2020**, *11*, 1369.
[3] J. Zhang, H. Yao, J. Mo, S. Chen, Y. Xie, S. Ma, R. Chen, T. Luo, W. Ling, L. Qin, Z. Wang, W. Zhou, *Nat. Commun.* **2022**, *13*, 5076.
[4] M. Wang, J. Zhang, R. Liu, T. Wu, W. Dai, R. Liu, J. Zhang, J. Liu, *IEEE Trans. Instrum. Meas.* **2023**, *72*, 9505711.
[5] H. Guo, X. Pu, J. Chen, Y. Meng, M.-H. Yeh, G. Liu, Q. Tang, B. Chen, D. Liu, S. Qi, *Sci. Rob.* **2018**, *3*, eaat2516.
[6] J. Yeom, A. Choe, S. Lim, Y. Lee, S. Na, H. J. S. a. Ko, *Sci. Adv.* **2020**, *6*, eaba5785.
[7] Y. Lee, J. Y. Oh, W. Xu, O. Kim, T. R. Kim, J. Kang, Y. Kim, D. Son, J. B.-H. Tok, M. Park, *Sci. Adv.* **2018**, *4*, eaat7387.
[8] N. Imam, T. A. Cleland, *Nat. Mach. Intell.* **2020**, *2*, 181.
[9] Y. H. Jung, S. K. Hong, H. S. Wang, J. H. Han, T. X. Pham, H. Park, J. Kim, S. Kang, C. D. Yoo, K. J. Lee, *Adv. Mater.* **2020**, *32*, 1904020.
[10] S. Gao, T. He, Z. Zhang, H. Ao, H. Jiang, C. Lee, *Adv. Sci.* **2021**, *8*, 2101834.
[11] W. Lin, B. Wang, G. Peng, Y. Shan, H. Hu, Z. Yang, *Adv. Sci.* **2021**, *8*, 2002817.
[12] C. Jiang, Z. Zhang, J. Pan, Y. Wang, L. Zhang, L. Tong, *Adv. Mater. Technol.* **2021**, *6*, 2100285.
[13] G. Li, S. Liu, L. Wang, R. Zhu, *Sci. Rob.* **2020**, *5*, eabc8134.
[14] C. M. Boutry, M. Negre, M. Jorda, O. Vardoulis, A. Chortos, O. Khatib, Z. Bao, *Sci. Rob.* **2018**, *3*, eaau6914.
[15] T. Chen, Q. Shi, M. Zhu, T. He, L. Sun, L. Yang, C. Lee, *ACS Nano* **2018**, *12*, 11561.
[16] T. He, Z. Sun, Q. Shi, M. Zhu, D. V. Anaya, M. Xu, T. Chen, M. R. Yuce, A. V.-Y. Thean, C. Lee, *Nano Energy* **2019**, *58*, 641.
[17] T. Yang, H. Pan, G. Tian, B. Zhang, D. Xiong, Y. Gao, C. Yan, X. Chu, N. Chen, S. Zhong, L. Zhang, W. Deng, W. Yang, *Nano Energy* **2020**, *72*, 104706.
[18] M.-O. Kim, S. Pyo, Y. Oh, Y. Kang, K.-H. Cho, J. Choi, J. Kim, *Smart Mater. Struct.* **2018**, *27*, 035001.
[19] J. H. Lee, J. S. Heo, Y. J. Kim, J. Eom, H. J. Jung, J. W. Kim, I. Kim, H. H. Park, H. S. Mo, Y. H. Kim, S. K. Park, *Adv. Mater.* **2020**, *32*, 2000969.
[20] S. Pyo, J. Lee, W. Kim, E. Jo, J. Kim, *Adv. Funct. Mater.* **2019**, *29*, 1902484.
[21] M. Zhu, Y. Yue, Y. Cheng, Y. Zhang, J. Su, F. Long, X. Jiang, Y. Ma, Y. Gao, *Adv. Electron. Mater.* **2020**, *6*, 1901064.
[22] M. Kang, J. Kim, B. Jang, Y. Chae, J.-H. Kim, J.-H. Ahn, *ACS Nano* **2017**, *11*, 7950.
[23] B. W. An, S. Heo, S. Ji, F. Bien, J.-U. Park, *Nat. Commun.* **2018**, *9*, 2458.
[24] A. A. Arriany, M. S. Musbah, in 2016 Int. Conf. on Engineering & MIS (ICEMIS), IEEE, Agadir, Morocco **2016**, pp. 1–6, https://doi.org/10.1109/ICEMIS.2016.7745292.
[25] P. K. Athira, C. J. Sruthi, A. Lijiya, *J. King Saud Univ. – Comput. Inf. Sci.* **2022**, *34*, 771.
[26] S. Shriram, B. Nagaraj, J. Jaya, S. Shankar, P. Ajay, *J. Healthcare Eng.* **2021**, *2021*, 8133076.
[27] Y. J. Tang, H. Zhou, X. P. Sun, N. H. Diao, J. B. Wang, B. S. Zhang, C. Qin, E. J. Liang, Y. C. Mao, *Adv. Funct. Mater.* **2020**, *30*, 9.
[28] K. Shrestha, S. Sharma, G. B. Pradhan, T. Bhatta, P. Maharjan, S. M. S. Rana, S. Lee, S. Seonu, Y. Shin, J. Y. Park, *Adv. Funct. Mater.* **2022**, *32*, 2113005.
[29] J. Cao, X. Fu, H. Zhu, Z. Qu, Y. Qi, Z. Zhang, Z. Zhang, G. Cheng, C. Zhang, J. Ding, *Small Methods* **2022**, *6*, 2200588.
[30] N. W. Bellono, D. B. Leitch, D. Julius, *Nature* **2017**, *543*, 391.
[31] Y. Zou, P. Tan, B. Shi, H. Ouyang, D. Jiang, Z. Liu, H. Li, M. Yu, C. Wang, X. Qu, L. Zhao, Y. Fan, Z. L. Wang, Z. Li, *Nat. Commun.* **2019**, *10*, 2695.
[32] G. von der Emde, M. Amey, J. Engelmann, S. Fetz, C. Folde, M. Hollmann, M. Metzen, R. Pusch, *J. Physiol. Paris* **2008**, *102*, 279.
[33] G. von der Emde, *J. Comp. Physiol., A* **2006**, *192*, 601.
[34] V. L. Salazar, R. Krahe, J. E. Lewis, *J. Exp. Biol.* **2013**, *216*, 2459.
[35] Q. Wang, H. Ding, X. Hu, X. Liang, M. Wang, Q. Liu, Z. Li, G. Sun, *Mater. Horiz.* **2020**, *7*, 2673.
[36] M. S. Sarwar, Y. Dobashi, C. Preston, J. K. M. Wyss, S. Mirabbasi, J. D. W. Madden, *Sci. Adv.* **2017**, *3*, 1602200.
[37] K. Zheng, F. Gu, H. Wei, L. Zhang, X. Chen, H. Jin, S. Pan, Y. Chen, S. Wang, *Small Methods* **2023**, *7*, 2201534.
[38] Q. Hua, J. Sun, H. Liu, R. Bao, R. Yu, J. Zhai, C. Pan, Z. L. Wang, *Nat. Commun.* **2018**, *9*, 244.
[39] Y. N. Zheng, Z. Yu, G. Mao, Y. Li, D. Pravarthana, W. Asghar, Y. Liu, S. Qu, J. Shang, R. W. Li, *Global Challenges* **2020**, *4*, 1900079.
[40] X. Liu, J. Liu, S. Lin, X. Zhao, *Mater. Today* **2020**, *36*, 102.
[41] K. Wang, X. Zhang, C. Li, X. Sun, Q. Meng, Y. Ma, Z. Wei, *Adv. Mater.* **2015**, *27*, 7451.
[42] Z. Zhao, H. Chen, H. Zhang, L. Ma, Z. Wang, *Biosens. Bioelectron.* **2017**, *91*, 306.
[43] F. Di Turo, P. Matricardi, C. Di Meo, F. Mazzei, G. Favero, D. Zane, *J. Cult. Heritage* **2019**, *37*, 113.
[44] K.-h. Zhu, X.-d. Han, S.-f. Ye, P.-x. Cui, L.-y. Dou, W.-b. Ma, S. Heng, X.-y. Tao, X.-y. Wei, *J. Energy Storage* **2022**, *53*, 105096.
[45] C. Yang, Z. Suo, *Nat. Rev. Mater.* **2018**, *3*, 125.
[46] H. R. Lee, C. C. Kim, J. Y. Sun, *Adv. Mater.* **2018**, *30*, 1704403.
[47] C.-C. Kim, H.-H. Lee, K. H. Oh, J.-Y. Sun, *Science* **2016**, *353*, 682.
[48] P. Yin, L. Tang, Z. Li, H. Guo, K. C. Aw, *Energy Convers. Manage.* **2023**, *278*, 116741.
[49] H. Nishiyama, M. Nakamura, *IEEE Trans. Compon., Packag., Manuf. Technol., Part A* **1994**, *17*, 477.
[50] A. Moin, A. Zhou, A. Rahimi, A. Menon, S. Benatti, G. Alexandrov, S. Tamakloe, J. Ting, N. Yamamoto, Y. Khan, F. Burghardt, L. Benini, A. C. Arias, J. M. Rabaey, *Nat. Electron.* **2020**, *4*, 54.
[51] S. Sundaram, P. Kellnhofer, Y. Li, J.-Y. Zhu, A. Torralba, W. Matusik, *Nature* **2019**, *569*, 698.
[52] Z. Zhang, Q. Shi, T. He, X. Guo, B. Dong, J. Lee, C. Lee, *Nano Energy* **2021**, *90*, 106517.